Bulletin of Mathematical Biology (2006)
DOI 10.1007/s11538-005-9055-7

ORIGINAL ARTICLE

A developmental model of ocular dominance column formation on a growing cortex

Andrew M. Oster*, Paul C. Bressloff

Department of Mathematics, University of Utah, Salt Lake City, UT 84112, United States of America

Received: date / Accepted: date

Abstract We derive an activity-based developmental model of ocular dominance column formation in primary visual cortex that takes into account cortical growth. The resulting evolution equation for the densities of feedforward afferents from the two eyes exhibits a sequence of pattern forming instabilities as the size of the cortex increases. We use linear stability analysis to investigate the nature of the transitions between successive patterns in the sequence. We show that these transitions involve the splitting of existing ocular dominance columns, such that the mean width of an OD column is approximately preserved during the course of development. This is consistent with recent experimental observations of postnatal growth in cat.

Keywords

1. Introduction

The primary visual cortex (V1) is characterized by a number of spatially distributed feature maps, in which local populations of neurons respond preferentially to stimuli with particular properties such as orientation and spatial frequency. Neurons also tend to respond more strongly to stimuli presented in one eye rather than the other, that is, they exhibit ocular dominance. Neurons sharing the same ocular dominance are grouped together into non-overlapping regions that form an alternating pattern of right and left eye preference across V1. Such regions have a characteristic periodicity and morphology that is species-dependent. For example, in the adult macaque monkey ocular dominance regions consist of branching stripes that have an approximately uniform width of 0.4 mm (Hubel and Wiesel, 1977) whereas in cat they are more patchy. An example of the ocular dominance

*Corresponding Address.

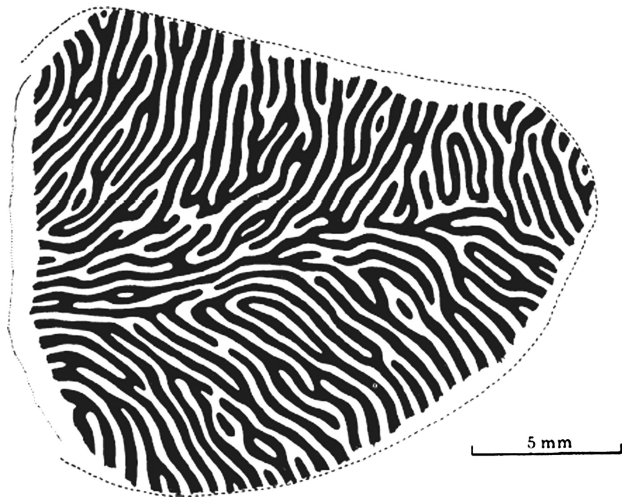

Fig. 1 Reconstruction of ocular dominance columns in primary visual cortex (V1) of macaque monkey shown in tangential section. Regions receiving input from one eye are shaded black and regions receiving input from the other eye are unshaded. The dashed line signifies the border between areas V1 and V2 (taken from Hubel and Wiesel, 1977).

pattern in macaque is shown in Fig. 1. In the case of cats (and ferrets), ocular dominance columns can be visualized at a very early postnatal stage (Crowley and Katz, 2000; Crair et al., 2001), during which the cortex is still undergoing significant growth. Indeed, Duffy et al. (1998) have shown that the surface area of adult cat V1 is more than double that of 1-week-old kittens, with the shape of V1 remaining unaltered. Although ocular dominance columns in macaque are fully formed at birth, the macaque brain undergoes a much smaller degree of postnatal growth (around 16%) (Purves and LaMantia, 1993). On the other hand, since ocular dominance columns are now formed prenatally, it is possible that they exist during a period of significant prenatal growth.

The large amount of postnatal growth in cat could have two very different effects on the spatial arrangement of ocular dominance columns. One possible scenario is that the ocular dominance map simply expands with the cortex, analogous to the expansion of a pattern drawn on the surface of a balloon. This would imply that the width of an ocular dominance column in an adult cat V1 is approximately double than that of a neonatal kitten. However, recent work by Rathjen et al. (2003) indicates that the spacing of adjacent ocular dominance columns in adults and kittens are approximately equal. This supports an alternative scenario in which new ocular dominance columns are added during postnatal growth in order to occupy the enlarged cortical surface. Since neurogenesis, neuronal migration and the ingrowth of thalamocortical afferents into the cortex have all ended by the third postnatal week in cats (Shatz and Luskin, 1986), it is likely that the addition of new columns would be achieved by the segregation of existing columns, rather than by the formation of completely new columns.

In this paper, we present an activity-based developmental model of ocular dominance column formation that takes into account cortical growth. In the case of a fixed cortical domain, our model reduces to the well-known Swindale model (Swindale, 1980, 1996), in which lateral cortical interactions consisting of short-range excitation and longer-range inhibition mediate a pattern forming instability with respect to the spatial distribution of feedforward afferents from the two eyes, resulting in alternating left and right eye dominated columns. The basic mechanism for the formation of ocular dominance columns in the Swindale model is analogous to the Turing instability in reaction–diffusion systems (Turing, 1952; Murray, 2002). That is, an initial spatially homogeneous state becomes unstable with respect to the growth of certain spatially periodic eigenmodes such that the period of the fastest growing mode determines the wavelength of the resulting pattern. It follows that the wavelength only depends on intrinsic properties of the system, such as the diffusion coefficients in a reaction–diffusion model or the range of lateral excitation and inhibition in the Swindale model. In the case of reaction–diffusion equations, the role of domain growth in pattern formation has recently been investigated by a number of authors (Painter et al., 1999; Varea et al., 1999; Chaplain et al., 2001). Much of this work has been inspired by experimental observations concerning the skin pigmentation of the marine angelfish (Kondo and Asai, 1995). In juvenile fish, the skin color is initially grey and then develops alternating white stripes on a dark blue background. New white stripes are inserted between the existing older stripes resulting in a doubling of the number of stripes each time the fish doubles in size. The nature of frequency-doubling transitions between quasi-steady-state reaction–diffusion patterns in a one-dimensional growing domain has been studied in some detail by Crampin et al. (1999, 2002). They show that frequency-doubling can occur either through activator peak insertions or through peak splitting. Moreover, a combination of the two in the form of frequency-tripling has been observed in a piecewise linear reaction–diffusion model with an additional inversion symmetry (Crampin et al., 2002). Motivated by the work on reaction–diffusion systems, we show in this paper that incorporating domain growth into a one-dimensional version of the Swindale model generates a sequence of quasi-steady-state patterns, in which existing ocular dominance columns segregate so that the approximate width of an OD column is preserved. We determine the transition points analytically by linearizing about the steady-state patterns, and show how this predicts very well the sequence of transitions observed numerically. The sequence of transitions appears similar in form to the frequency-tripling transitions identified by Crampin et al. (2002), although the mechanism for transitions between steady-state patterns is very different from the reaction–diffusion case. The occurrence of frequency-tripling rather than frequency-doubling reflects the underlying exchange symmetry between left and right ocular dominance columns.

An important implication of our analysis is that in order for new ocular dominance columns to occur, it is necessary that the lateral interactions are themselves nontrivially modified during cortical growth. That is, a simple elongation of the lateral interactions as the cortex grows will not induce any pattern transitions. Interestingly, this observation is consistent with recent experimental studies concerning the development of patchy long-range connections in cortex (Schmidt et al., 1999).

These connections form a reciprocal system of axon collaterals that arborize at regular distances of about 1 mm and link cells with similar feature preferences such as ocular dominance. It follows that if the approximate size of an ocular dominance column is preserved during postnatal cortical growth, then the distance between patches should also be preserved, most likely through the refinement of existing clusters. There is experimental evidence that the long-range connections do undergo both elongation and refinement postnatally (Luhmann et al., 1990; Callaway and Katz, 1991). For simplicity, rather than explicitly modeling the refinement of long-range connections, we introduce a scaling rule for the lateral interactions.

Finally, note that independently of the issue of cortical growth, this paper presents for the first time analytical results regarding the stability of ocular dominance patterns. Our analysis not only applies to the original Swindale model but also to the well-known correlation-based Hebbian model of Miller et al. (1989), which exhibits very similar behavior. Previous analytical studies of these and related models have focused on the linear eigenmodes associated with the growth from a binocular state rather than the stability of the final nonlinear pattern (Swindale, 1980, 1996; Miller et al., 1989). It is generally not possible to analyze the stability of the patterns by carrying out a perturbation expansion about the binocular state, since the Turing instability appears to be subcritical, in the sense that large amplitude patterns are formed just beyond the bifurcation point. However, classical bifurcation techniques could be applicable to other classes of developmental model that exhibit smooth transitions to ocular dominance column patterns (see, e.g., Harris et al., 2000), with stripe insertions occurring via secondary bifurcations (Ermentrout and Cowan, 1980).

2. Developmental model on a growing domain

In this section, we construct an extension of the Swindale model of ocular dominance column formation (Swindale, 1980) that takes into account cortical growth. We proceed along analogous lines to the recent study of reaction–diffusion systems on a growing domain by Crampin et al. (1999, 2002). The Swindale model treats input layer 4 of cortex as a two-dimensional sheet of neural tissue and considers competition between the synaptic densities of feedforward afferents from the left and right eyes that are relayed from the lateral genciculate nucleus (LGN) of the thalamus. Such competition is mediated by lateral interactions across cortex. Let $n_{\mathrm{L}}(\mathbf{r}, t)$ and $n_{\mathrm{R}}(\mathbf{r}, t)$ denote the densities of left and right eye synaptic connections to a point $\mathbf{r} = (x, y)$ on cortex at time t. For the moment we treat the two-dimensional cortical domain Ω as fixed (no cortical growth). The feedforward synaptic weights evolve according to the equation (Swindale, 1980)

$$\frac{\partial n_i(\mathbf{r}, t)}{\partial t} = \left[\sum_{j=\mathrm{R,L}} \int_{\Omega} w_{ji}(|\mathbf{r}' - \mathbf{r}|) n_j(\mathbf{r}', t)\, \mathrm{d}\mathbf{r}' \right] F(n_i(\mathbf{r}, t)) \tag{1}$$

for $i = \mathrm{R}, \mathrm{L}$. The logistic function $F(n_i) = n_i(N - n_i)$ ensures that the growth of n_i terminates at a maximum density N and that the weights remain positive, that is,

$0 \leq n_i \leq N$. Same-eye lateral interactions w_{RR} and w_{LL} are assumed to be positive for small cortical separations $|\mathbf{r} - \mathbf{r}'|$ (short-range excitation) and negative for large cortical separations (long-range inhibition). The opposite-eye interactions w_{RL} and w_{LR} are assumed to be anti-correlated, in the sense that they consist of short-range inhibition and long-range excitation.[1] As a further simplification, suppose that the total synaptic weight at any point in cortex is constant with $n_L + n_R = N$. This condition implies $\partial n_R/\partial t = -\partial n_L/\partial t$, which is guaranteed if the eyes are symmetrically anti-correlated, $w_{RR} = -w_{RL}$ and $w_{LL} = -w_{LR}$. We introduce a new normalized density variable $n = (n_L - n_R)/N$, which determines the ocular dominance at each point $\mathbf{r}$. In particular, $n = 0$ corresponds to a binocular state and $n = 1$ ($n = -1$) corresponds to a monocular state with complete left (right) eye dominance. The system (1) then reduces to the scalar integro-differential equation

$$\frac{\partial n(\mathbf{r}, t)}{\partial t} = [1 - n(\mathbf{r}, t)^2]\left[\int_\Omega w(|\mathbf{r} - \mathbf{r}'|)n(\mathbf{r}', t)\, d\mathbf{r}' + K(\mathbf{r})\right], \tag{2}$$

where $w = (N/2)^2[w_{RR} + w_{LL}]$ and $K(\mathbf{r}) = (N/2)^2 \int_\Omega [w_{LL}(|\mathbf{r}' - \mathbf{r}|) - w_{RR}(|\mathbf{r}' - \mathbf{r}|)]\, d\mathbf{r}'$, which reduces to a constant in the unbounded domain $\Omega = \mathbb{R}^2$. We will assume that the interactions are symmetric with respect to interchange of the two eyes ($w_{LL} = w_{RR}$) so that $K = 0$. Swindale (1980) showed how competition between short-range excitation and long-range inhibition can induce a Turing-like instability of the binocular equilibrium solution of Eq. (2), leading to the spontaneous formation of ocular dominance columns. Moreover, the morphology of the resulting stripe pattern is consistent with experimentally determined ocular dominance columns in primates.

In order to extend the Swindale model to the case of a growing cortex, we rewrite it in the integral form

$$\frac{d}{dt}\int_{\Omega_t} n(\mathbf{r}, t)\, d\mathbf{r} = \int_{\Omega_t} \mathcal{F}_t[n](\mathbf{r}, t)\, d\mathbf{r}, \tag{3}$$

where Ω_t is the cortical domain at time t and (for $K = 0$)

$$\mathcal{F}_t[n](\mathbf{r}, t) = [1 - n(\mathbf{r}, t)^2]\left[\int_{\Omega_t} w_t(|\mathbf{r} - \mathbf{r}'|)n(\mathbf{r}', t)\, d\mathbf{r}'\right]. \tag{4}$$

[1] The lateral interactions in the Swindale model are a phenomenological representation of a number of different forms of interaction. These include statistical correlations between feedforward inputs from the thalamus, short-range and long-range intracortical synaptic connections, and possibly the diffusion of secondary messenger molecules. The reversal in sign of opposite eye interactions is supposed to reflect negative statistical correlations between left and right eye inputs. However, the existence of negative correlations is difficult to justify from a neurobiological perspective. The problem of negative correlations can be avoided by using a linear Hebbian model with subtractive normalization instead of the Swindale model (Miller et al., 1989). It turns out that both models exhibit very similar behavior and can be analyzed in almost an identical fashion. The relationship between the two models will be discussed further in Section 5.

The subscript t indicates that the lateral interaction function w_t may vary with the size of the cortex. Using the Reynolds transport theorem to evaluate the left-hand side,

$$\frac{\mathrm{d}}{\mathrm{d}t}\int_{\Omega_t} n(\mathbf{r},t)\,\mathrm{d}\mathbf{r} = \int_{\Omega_t}\left[\frac{\partial n}{\partial t} + \nabla\cdot(\mathbf{u}(t)n(\mathbf{r},t))\right]\mathrm{d}\mathbf{r}, \tag{5}$$

where $\mathbf{u}(t)$ is the flow of the domain at time t, we obtain the evolution equation

$$\frac{\partial n}{\partial t} + \nabla\cdot(\mathbf{u}n) = \mathcal{F}_t[n]. \tag{6}$$

The growing domain Ω_t introduces an advection term $\mathbf{u}\cdot\nabla n$, indicating that the feedforward afferents attached to the cortex move with the cortex, and a dilution term $n\nabla\cdot\mathbf{u}$ that takes into account changes in surface area of cortex. Following Crampin et al. (1999), we specify the growth of the cortex using a Lagrangian description:

$$\mathbf{r} = \Gamma(\mathbf{R},t), \quad \mathbf{r}\in\Omega_t, \quad \mathbf{R}\in\Omega_0, \tag{7}$$

where $\mathbf{R}$ is the point at time $t=0$ that maps to the point $\mathbf{r}$ at time t according to the growth function Γ. Note that $\Gamma(\mathbf{R},0)=\mathbf{R}$. The velocity field for the flow is then given by

$$\mathbf{u}(\mathbf{r},t) = \frac{\partial \mathbf{r}}{\partial t} = \frac{\partial \Gamma}{\partial t} \tag{8}$$

for fixed $\mathbf{R}$. On the basis of the experimental work of Duffy et al. (1998), who showed that between postnatal weeks 3 and 6 cat V1 undergoes a uniform expansion in which it approximately doubles in size, we assume that the growth is slow and isotropic. It should be noted that our extension of the Swindale model is formulated in terms of the normalized synaptic density $n=(n_\mathrm{L}-n_\mathrm{R})/N$ where $N=n_\mathrm{L}+n_\mathrm{R}$ is the fixed total density at each point in cortex. This implies that the total number of synapses is itself time-dependent, growing in proportion to the total surface area of cortex. That is, $N_\mathrm{Tot}(t)\equiv\int_{\Omega_t}[n_\mathrm{L}(\mathbf{r})+n_\mathrm{R}(\mathbf{r})]\,\mathrm{d}\mathbf{r} = N\Omega_t$. It is usually assumed that the development of ocular dominance columns involves the rearrangement or pruning of existing connections, which would imply that the total number of afferent connections remains the same or actually decreases. On the other hand, it is also possible that the strength or efficacy of the remaining connections actually increases through the formation of more extensive arborizations. Since our simple developmental model does not distinguish between the number of synapses and their strength, it is not clear how best to model any variation of N with cortical growth. Given that such a variation simply introduces an additional slowly varying term in the dynamical equations and this does not affect the basic pattern formation process, we will treat N as fixed.

In this paper, we further restrict ourselves to the simpler case of a one-dimensional cortical domain $\Omega_t=[0,L(t)]$ where $L(t)$ is the size of the cortex at

time t. Isotropic flow can then be written in the form

$$\Gamma(X,t) = X\rho(t), \quad \rho(0) = 1 \tag{9}$$

with corresponding velocity field

$$u(x,t) = X\dot{\rho} = x\frac{\dot{\rho}}{\rho}. \tag{10}$$

The size of cortex grows as $L(t) = L_0\rho(t)$. Substitution into the one-dimensional version of Eq. (6) gives

$$\frac{\partial n}{\partial t} + \left(\frac{\dot{\rho}}{\rho}\right)\left(x\frac{\partial n}{\partial x} + n\right) = \mathcal{F}_t[n], \tag{11}$$

with

$$\mathcal{F}_t[n](x,t) = [1 - n(x,t)^2]\left[\int_0^{L(t)} w_t(|x - x'|)n(x',t)\,\mathrm{d}x'\right]. \tag{12}$$

Following Crampin et al. (1999), we transform Eq. (11) to the fixed interval $[0, L_0]$ by performing the change of variables

$$(x,t) \to (\bar{x},\bar{t}) = \left(\frac{x}{\rho(t)}, t\right). \tag{13}$$

Under this transformation the advection term in Eq. (11) is eliminated, since

$$\frac{\partial n}{\partial \bar{t}} = \frac{\partial n}{\partial t} + x\frac{\dot{\rho}}{\rho}\frac{\partial n}{\partial x}.$$

On dropping the overbars, we obtain the modified evolution equation

$$\frac{\partial n}{\partial t} = \widehat{\mathcal{F}}_t[n] - n\frac{\dot{\rho}}{\rho}, \tag{14}$$

where

$$\widehat{\mathcal{F}}_t[n](x,t) = \rho(t)[1 - n(x,t)^2]\left[\int_0^{L_0} w_t(|x - x'|\rho(t))n(x',t)\,\mathrm{d}x'\right]. \tag{15}$$

It remains to specify more explicitly the form of the lateral interaction function w_t and how it scales with time t. As in the original Swindale model (Swindale, 1980), we require that the lateral interactions mediate competition through short-range excitation and long-range inhibition. Therefore, we introduce a "Mexican hat" function given by a difference-of-exponentials

$$W(x) = A\left[\mathrm{e}^{-\sigma_{\mathrm{E}}|x|} - \beta \mathrm{e}^{-\sigma_{\mathrm{I}}|x|}\right] \tag{16}$$

with $A > 0, 0 < \beta < 1$ and $\sigma_{\mathrm{E}} > \sigma_{\mathrm{I}}$. Here $\sigma_{\mathrm{E}}, \sigma_{\mathrm{I}}$ are space constants that determine the range of excitation and inhibition. (One could equally well take $W(x)$ to be a difference-of-Gaussians; we consider exponential functions for analytical convenience.) Given the function $W(x)$, we assume the following scaling behavior for the lateral interaction function w_t:

$$w_t(x) = \gamma_1(t) W(\gamma_2(t)x) \tag{17}$$

If the lateral interactions simply grow with the cortex (the "balloon effect") then $\gamma_1(t) = \gamma_2(t) = 1/\rho(t)$, which takes into account both the local expansion of cortex and the increase in the range of interactions, that is, $\sigma_{\mathrm{E,I}} \to \sigma_{\mathrm{E,I}}/\rho(t)$. Equation (14) then reduces to the form

$$\frac{\partial n}{\partial t} = \mathcal{F}_0[n] - n\frac{\dot{\rho}}{\rho}.$$

In this case, the only effect of cortical growth is the addition of a dilution term $n\dot{\rho}/\rho$, which will be small for slow growth. If this term is dropped then we recover the original Swindale model on a fixed domain of size L_0; this cannot exhibit a sequence of pattern forming instabilities in which new ocular dominance columns are added as the cortex grows. Therefore, we require that the lateral interactions undergo some refinement as the cortex grows that is beyond simple expansion. It is difficult to determine from first principles the form of such a refinement, since the lateral interactions in the Swindale model are a phenomenological representation of a number of different forms of interaction. Here we make the ansatz that $\gamma_1(t) = \gamma_2(t) = 1$, which corresponds to taking the distribution of lateral interactions to be invariant with respect to cortical growth. Equation (14) then becomes

$$\frac{\partial n}{\partial t} = \rho(t)[1 - n(x,t)^2]\left[\int_0^{L_0} W(|x - x'|\rho(t))n(x',t)\,\mathrm{d}x'\right] - n\frac{\dot{\rho}}{\rho}. \tag{18}$$

In order to simplify our analysis we will drop the dilution term $n\dot{\rho}/\rho$, which is motivated by the fact that $\dot{\rho}$ is small for slow growth. This then allows us to consider the existence and stability of steady-state solutions of the form $n(x) = \pm 1$ for all $0 \le x \le L_0$ (see Section 3). Numerically, we find that such an approximation does not alter our main results (see Section 4). Incorporating an explicit dynamics for the growth rate ρ, we finally obtain the pair of equations

$$\frac{\partial n}{\partial t} = [1 - n(x,t)^2]\left[\int_0^{L_0} W_\rho(|x - x'|)n(x',t)\,\mathrm{d}x'\right], \tag{19}$$

$$\frac{\partial \rho}{\partial t} = \varepsilon f(\rho), \tag{20}$$

where

$$W_\rho(x) = \rho W(\rho x). \tag{21}$$

Since the growth of cortex saturates in the adult, we assume logistic growth by taking (Crampin et al., 1999)

$$f(\rho) = \rho\,(1 - \rho/\xi)\,, \tag{22}$$

so that

$$\rho(t) = \frac{\mathrm{e}^{\epsilon t}}{1 + \xi^{-1}(\mathrm{e}^{\epsilon t} - 1)}. \tag{23}$$

Here ξ is the ratio of initial to final lengths, that is, $\lim_{t\to\infty} \rho(t) = \xi$. Equations (19) and (20) generate a sequence of patterns in time. For slow growth $\varepsilon \ll 1$, we can identify two distinct dynamical regimes along analogous lines to the reaction diffusion system of Crampin et al. (1999). If $\partial n/\partial t \ll 1/\varepsilon$ then n evolves to a quasi-steady-state pattern of alternating ocular dominance columns that is modulated by the slowly varying parameter ρ. However, when $\partial n/\partial t = \mathcal{O}(1/\varepsilon)$ quasi-stationarity is lost, signaling the onset of a fast transition to the next pattern in the sequence. Such a transition arises because of destabilization of an existing pattern when ρ reaches a critical value. Moreover, as we establish in Section 3, the nature of the transition between successive patterns can be understood by considering the growth of linear eigenmodes close to the point of instability. In particular, away from the boundary we find frequency-tripling, in which each ocular dominance column splits into three alternating columns. The occurrence of frequency-tripling rather than frequency-doubling reflects the fact that the Swindale model is symmetric with respect to the exchange of left and right eye ocular dominance columns. This is analogous to the inversion symmetry required for the observation of frequency-tripling in a piecewise linear reaction–diffusion system (Crampin et al., 2002).

3. Linear stability analysis on a fixed domain

The basic mechanism for ocular dominance columns formation originally proposed by Swindale (1980) involves the growth of spatially periodic eigenmodes from the homogeneous binocular state $n(x) = 0$ for all $x \in \Omega$ where Ω is a fixed domain. Linearizing about the binocular state gives

$$\frac{\partial n(x,t)}{\partial t} = \int_\Omega W(|x - x'|)n(x',t)\,\mathrm{d}x'. \tag{24}$$

Suppose, for the moment, that $\Omega = \mathbb{R}$. The solutions of (24) are then of the form $n(x,t) = \mathrm{e}^{\lambda t}\mathrm{e}^{ik\cdot k}$ and the growth factor λ satisfies the dispersion relation

$$\lambda = \widetilde{W}(k) \equiv \int_{-\infty}^{\infty} \mathrm{e}^{ikx} W(|x|)\,\mathrm{d}x. \tag{25}$$

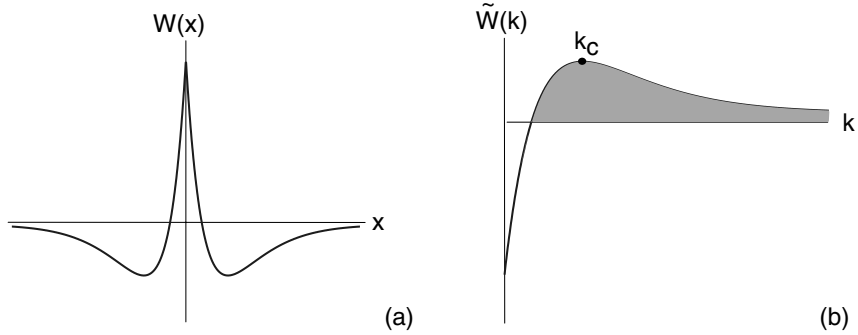

Fig. 2 (a) Difference-of-exponentials interaction function $W(x)$ displaying short-range excitation and long-range inhibition. (b) Fourier transform $\widetilde{W}(k)$ with maximum at $k = k_c$. The gray shaded region denotes the semi-infinite band of unstable modes.

Thus, the rate of growth or decay of the linear eigenmodes is determined by the Fourier transform $\widetilde{W}$ of the lateral interaction function W. An example of a difference-of-exponentials function $W(x)$ and its transform $\widetilde{W}(k)$ are plotted in Fig. 2 for the case $\widetilde{W}(0) < 0$. It can be seen that there is a semi-infinite band of eigenmodes that are unstable (positive λ). The value of k that maximizes $\widetilde{W}(k)$ is called the critical wavenumber k_c. One finds numerically that the critical wave number k_c determines the approximate wavelength of the pattern that emerges from the homogeneous initial state (or some random initial state). The resulting pattern consists of alternating left and right ocular dominance columns with approximate width π/k_c and with sharp boundaries (Swindale, 1980). The mechanism for the formation of such a pattern is analogous to the Turing instability of reaction–diffusion systems (Turing, 1952; Murray, 2002), where competition is mediated by diffusing and reacting chemical species rather than nonlocal lateral interactions.

Figure 2 is oversimplified, in the sense that it does not take into account boundary effects. Nevertheless, we will assume that at some critical point in development, ocular dominance columns spontaneously emerge through a Turing-like instability from a binocular state. For concreteness, suppose that this occurs when $\rho = 1$, that is, the cortex has size L_0. Of course, the initial development of ocular dominance itself takes time so that one cannot really ignore the growth of the cortex during this period. However, we assume that this does not have a significant effect on the initial Turing instability. Once the ocular dominance pattern has formed, the cortex continues to grow, that is, ρ increases. At some critical value of ρ the pattern becomes unstable and a new pattern is formed. This can be understood in terms of a state transition between two patterns belonging to the class of steady-state solutions:

$$\bar{n}(x) = \begin{cases} 1, & \text{for} \quad x \in \Sigma_+ \\ -1, & \text{for} \quad x \in \Sigma_- \end{cases} \tag{26}$$

with $\Sigma_\pm \subset [0, L_0]$ such that $\Sigma_+ \cup \Sigma_- = [0, L_0]$. Here Σ_+ (Σ_-) signifies the subregion spanned by the left-eye (right-eye) ocular dominance columns. Although the existence of these solutions is independent of ρ, their stability properties strongly depend on ρ. Linearizing Eq. (19) about $\bar{n}(x)$ by setting $n(x,t) = \bar{n}(x) + c(x,t)$ and expanding to first order in c gives

$$\frac{\partial c(x,t)}{\partial t} = -2\Lambda_\rho(x)\bar{n}(x)c(x,t), \tag{27}$$

where

$$\Lambda_\rho(x) = \int_0^{L_0} W_\rho(|x-x'|)\bar{n}(x')\,\mathrm{d}x'. \tag{28}$$

The condition for (marginal) stability of the equilibrium solution $\bar{n}$ is then

$$\Lambda_\rho(x) \begin{cases} \geq 0, & \text{for} \quad x \in \Sigma_+ \\ \leq 0, & \text{for} \quad x \in \Sigma_- \end{cases}. \tag{29}$$

In the following, we determine Λ_ρ and its dependence on ρ for some simple examples of stationary solutions satisfying Eq. (26) including fronts, single bumps and periodic patterns. We use this to gain insights into the nature of the growth-induced transition between successive ocular dominance patterns. In particular, we show that frequency-tripling tends to occur away from the boundary.

3.1. Stationary front

Consider the stationary front solution

$$\bar{n}(x) = \begin{cases} -1, & 0 \leq x < x_0 \\ 1, & x_0 < x \leq L_0 \end{cases} \tag{30}$$

with $0 < x_0 < L_0$. The corresponding function Λ_ρ defined by Eq. (28) takes the form

$$\Lambda_\rho(x) = \int_{x_0}^{L_0} W_\rho(|x-x'|)\,\mathrm{d}x' - \int_0^{x_0} W_\rho(|x-x'|)\,\mathrm{d}x'. \tag{31}$$

Substituting for W_ρ using Eqs. (16) and (21) gives

$$\Lambda_\rho(x) = \rho\left[\Phi_{\hat{\sigma}_\mathrm{E}}(x) - \beta\Phi_{\hat{\sigma}_\mathrm{I}}(x)\right] \tag{32}$$

with $\hat{\sigma}_{\mathrm{E,I}} = \rho\sigma_{\mathrm{E,I}}$ and

$$\Phi_\sigma(x) = \int_{x_0}^{L_0} \mathrm{e}^{-\sigma|x-x'|}\,\mathrm{d}x' - \int_0^{x_0} \mathrm{e}^{-\sigma|x-x'|}\,\mathrm{d}x'. \tag{33}$$

Evaluating the integrals shows that

$$\Phi_\sigma(x) = \begin{cases} \Phi_\sigma^-(x), & 0 \le x < x_0 \\ \Phi_\sigma^+(x), & x_0 < x \le L_0 \end{cases} \tag{34}$$

with

$$\Phi_\sigma^+(x) = \frac{1}{\sigma}\left[2 - 2\mathrm{e}^{-\sigma(x-x_0)} - \mathrm{e}^{-\sigma(L_0-x)} + \mathrm{e}^{-\sigma x}\right], \tag{35}$$

and

$$\Phi_\sigma^-(x) = \frac{1}{\sigma}\left[2\mathrm{e}^{\sigma(x-x_0)} - 2 - \mathrm{e}^{-\sigma(L_0-x)} + \mathrm{e}^{-\sigma x}\right]. \tag{36}$$

The general stability condition (29) implies that the stationary front is stable if $\Lambda_\rho(x) \le 0$ for all $0 \le x < x_0$ and $\Lambda_\rho(x) \ge 0$ for all $x_0 < x \le L_0$. Since $\Lambda_\rho(x)$ is a continuous function of x, it follows that a necessary condition for a stable front is $\Lambda_\rho(x_0) = 0$. Combining this with Eqs. (32), (41), (35) and (36), we obtain the stability condition

$$\frac{1}{\sigma_\mathrm{E}}\mathrm{e}^{-x_0\hat{\sigma}_\mathrm{E}} - \frac{\beta}{\sigma_\mathrm{I}}\mathrm{e}^{-\hat{\sigma}_\mathrm{I}x_0} = \frac{1}{\sigma_\mathrm{E}}\mathrm{e}^{-\hat{\sigma}_\mathrm{E}(L_0-x_0)} - \frac{\beta}{\sigma_\mathrm{I}}\mathrm{e}^{-\hat{\sigma}_\mathrm{I}(L_0-x_0)}. \tag{37}$$

The latter is satisfied if $x_0 = L_0/2$ independently of the parameters β, $\sigma_{\mathrm{E,I}}$ and ρ. Therefore, we will take $x_0 = L_0/2$ in the following. (Note that for certain ranges of parameters there can exist other solutions x_0 of Eq. (37), but the corresponding fronts tend to be unstable.)

In Fig. 3, we plot $\Lambda_\rho(x)$ for a range of values of ρ with $x_0 = 1/2$, $L_0 = 1$ and fixed weight parameters $\sigma_{\mathrm{E,I}}$, β. Note that $\Lambda_\rho(x)$ is an odd function with respect to reflections about $x = 1/2$, that is, $\Lambda_\rho(1-x) = \Lambda_\rho(x)$ for $0 \le x \le 1/2$. The front is stable provided that the function $\Lambda_\rho(x)$ only crosses the x-axis at the

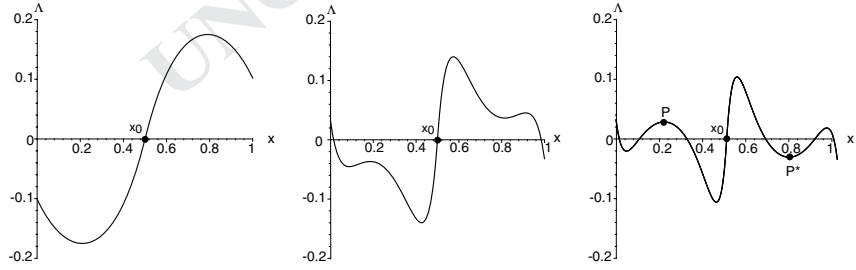

Fig. 3 Plot of $\Lambda_\rho(x)$ for various values of the scale factor ρ in the case of a stationary front with center at $x_0 = 1/2$ for $L_0 = 1$. The parameters of the weight distribution (16) are taken to be $\beta = 0.5$, $\sigma_\mathrm{E} = 4.4$, $\sigma_\mathrm{I} = 1.9$ and $A = 10$. (a) $\rho = 1$: front solution is stable since $\Lambda_\rho(x) < 0$ for $0 \le x < 1/2$ and $\Lambda_\rho(x) > 0$ for $x_0 < x \le 1$. (b) $\rho = 4$: front solution is unstable since $\Lambda_\rho(x)$ crosses the x-axis close to the boundary of the domain. The function $\Lambda_\rho(x)$ also develops additional extrema. (c) $\rho = 6$: additional regions of instability occur due to the extrema at P, P^* crossing the x-axis.

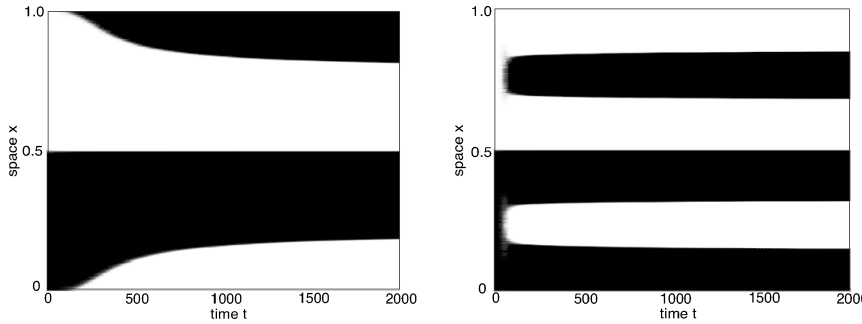

Fig. 4 Evolution of an unstable stationary front for fixed ρ. Other parameter values as in Fig. 3. (a) $\rho = 4$: insertion of new columns at the boundary. (b) $\rho = 6$: frequency-tripling in which each column splits into three alternating columns.

point $x = 1/2$. It can be seen that as ρ increases, zero crossings occur close to the boundary of the domain. The function $\Lambda_\rho(x)$ also develops additional stationary points so that as ρ is further increased, these points also cross the x-axis leading to additional regions of instability. It is these latter crossings that generate the splitting of ocular dominance columns via frequency-tripling. In order for this to be the primary instability, however, the zero crossings at the boundary have to be suppressed. Otherwise, the front destabilizes with respect to the zero crossings close to the boundary leading to the insertion of new columns at the boundary rather than frequency-tripling. This is illustrated in Fig. 4, where we show the evolution of an unstable front for the fixed values of ρ corresponding to Fig. 3(b,c). One way to remove the boundary instability would be to introduce periodic boundary conditions, as shown in Section 4. It turns out that the basic transitions identified for the front carry over to the case of single or multiple bump solutions (see below). Hence, if boundary effects are suppressed or negligible (as when starting from a large number of bumps) then increasing ρ leads to a sequence of frequency-tripling transitions. On the other hand, if boundary effects are significant then the sequence of transitions is more irregular.

3.2. Single stationary bump

Let us now consider a stationary bump solution of the form

$$\bar{n}(x) = \begin{cases} -1, & 0 \le x < x_0 \\ 1, & x_0 < x \le x_1 \\ -1, & x_1 < x < L_0 \end{cases} \tag{38}$$

with $0 < x_0 < x_1 < L_0$. (The bump is the region where $\bar{n} = +1$.) The corresponding function Λ_ρ defined by Eq. (28) takes the form

$$\Lambda_\rho(x) = -\int_0^{x_0} W_\rho(|x - x'|)\,dx' + \int_{x_0}^{x_1} W_\rho(|x - x'|)\,dx' - \int_{x_1}^{L_0} W_\rho(|x - x'|)\,dx'. \tag{39}$$

340 Substituting for W_ρ using Eqs. (16) and (21) gives Eq. (32) with

$$\Phi_\sigma(x) = -\int_0^{x_0} \mathrm{e}^{-\sigma|x-x'|}\mathrm{d}x' + \int_{x_0}^{x_1} \mathrm{e}^{-\sigma|x-x'|}\mathrm{d}x' - \int_{x_1}^{L_0} \mathrm{e}^{-\sigma|x-x'|}\mathrm{d}x'. \tag{40}$$

341 Evaluating the integrals shows that

$$\Phi_\sigma(x) = \begin{cases} \Phi_\sigma^-(x), & 0 \le x < x_0 \\ \Phi_\sigma^0(x), & x_0 \le x < x_1 \\ \Phi_\sigma^+(x), & x_1 < x \le L_0 \end{cases} \tag{41}$$

with

$$\Phi_\sigma^+(x) = \frac{1}{\sigma}\left[\mathrm{e}^{-\sigma x} - 2\mathrm{e}^{-\sigma(x-x_0)} + 2\mathrm{e}^{-\sigma(x-x_1)} - 2 + \mathrm{e}^{-\sigma(L_0-x)}\right], \tag{42}$$

$$\Phi_\sigma^0(x) = \frac{1}{\sigma}\left[\mathrm{e}^{-\sigma x} - 2\mathrm{e}^{-\sigma(x-x_0)} - 2\mathrm{e}^{\sigma(x-x_1)} + 2 + \mathrm{e}^{-\sigma(L_0-x)}\right], \tag{43}$$

342 and

$$\Phi_\sigma^-(x) = \frac{1}{\sigma}\left[\mathrm{e}^{-\sigma x} + 2\mathrm{e}^{\sigma(x-x_0)} - 2\mathrm{e}^{\sigma(x-x_1)} - 2 + \mathrm{e}^{-\sigma(L_0-x)}\right]. \tag{44}$$

The general stability condition (29) implies that the stationary bump is stable if $\Lambda_\rho(x) \le 0$ for $0 \le x < x_0$, $x_1 < x \le L_0$ and $\Lambda_\rho(x) \ge 0$ for $x_0 < x < x_1$. Since $\Lambda_\rho(x)$ is a continuous function of x, it follows that a necessary condition for a stable bump is $\Lambda_\rho(x_0) = \Lambda_\rho(x_1) = 0$. Combining this with Eqs. (32), (41), (42), (43) and (44), we obtain the stability conditions

$$\frac{1}{\sigma_\mathrm{E}}\left[\mathrm{e}^{-\hat{\sigma}_\mathrm{E}x_0} + \mathrm{e}^{-\hat{\sigma}_\mathrm{E}(L_0-x_0)} - 2\mathrm{e}^{-\hat{\sigma}_\mathrm{E}(x_1-x_0)}\right]$$
$$\times = \frac{\beta}{\sigma_\mathrm{I}}\left[\mathrm{e}^{-\hat{\sigma}_\mathrm{I}x_0} + \mathrm{e}^{-\hat{\sigma}_\mathrm{I}(L_0-x_0)} - 2\mathrm{e}^{-\hat{\sigma}_\mathrm{I}(x_1-x_0)}\right], \tag{45}$$

and

$$\frac{1}{\sigma_\mathrm{E}}\left[\mathrm{e}^{-\hat{\sigma}_\mathrm{E}x_1} + \mathrm{e}^{-\hat{\sigma}_\mathrm{E}(L_0-x_1)} - 2\mathrm{e}^{-\hat{\sigma}_\mathrm{E}(x_1-x_0)}\right]$$
$$= \frac{\beta}{\sigma_\mathrm{I}}\left[\mathrm{e}^{-\hat{\sigma}_\mathrm{I}x_1} + \mathrm{e}^{-\hat{\sigma}_\mathrm{I}(L_0-x_1)} - 2\mathrm{e}^{-\hat{\sigma}_\mathrm{I}(x_1-x_0)}\right]. \tag{46}$$

Equations (45) and (46) can be reduced to a single equation for the intersection point x_0 in the particular case $x_1 = L_0 - x_0$:

$$\frac{1}{\sigma_\mathrm{E}}\left[\mathrm{e}^{-\hat{\sigma}_\mathrm{E}x_0} + \mathrm{e}^{-\hat{\sigma}_\mathrm{E}(L_0-x_0)} - 2\mathrm{e}^{-\hat{\sigma}_\mathrm{E}(L_0-2x_0)}\right]$$
$$= \frac{\beta}{\sigma_\mathrm{I}}\left[\mathrm{e}^{-\hat{\sigma}_\mathrm{I}x_0} + \mathrm{e}^{-\hat{\sigma}_\mathrm{I}(L_0-x_0)} - 2\mathrm{e}^{-\hat{\sigma}_\mathrm{I}(L_0-2x_0)}\right], \tag{47}$$

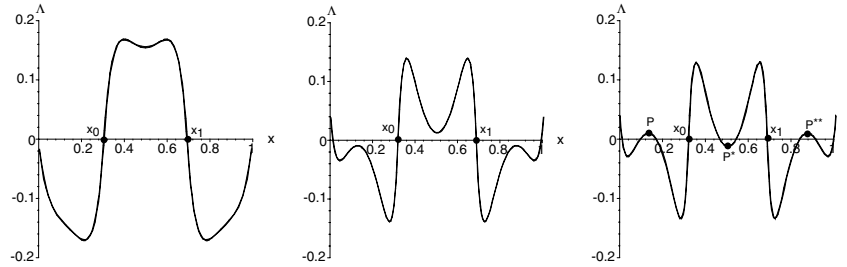

Fig. 5 Plot of $\Lambda_\rho(x)$ for various values of the scale factor ρ in the case of a stationary bump with jumps at x_0, x_1 for $L_0 = 1$. The parameters of the weight distribution (16) are as in Fig. 3. (a) $\rho = 4$: bump solution is stable since $\Lambda_\rho(x) < 0$ for $x \in (0, x_0) \cup (x_1, 1)$ and $\Lambda_\rho(x) > 0$ for $x \in (x_0, x_1)$. (b) $\rho = 7.2$: bump solution is unstable since $\Lambda_\rho(x)$ crosses the x-axis close to the boundary of the domain. The function $\Lambda_\rho(x)$ also develops additional extrema. (c) $\rho = 8$: additional regions of instability occur because of the extrema at P, P^*, P^{**} crossing the x-axis.

One can then obtain an approximate solution to Eq. (47) in the large-ρ limit. First, recall that $\hat{\sigma}_{\mathrm{E,I}} = \rho\sigma_{\mathrm{E,I}}$. Since $\sigma_{\mathrm{E}} > \sigma_{\mathrm{I}}$, it follows that each term on the left-hand side is much smaller than the corresponding term on the right-hand side and can be neglected. Taking $x_0 = 1/3 - \delta$ then leads to the following equation

$$\mathrm{e}^{-\hat{\sigma}_1/3}\mathrm{e}^{\hat{\sigma}_1\delta} + \mathrm{e}^{-2\hat{\sigma}_1/3}\mathrm{e}^{-\hat{\sigma}_1\delta} - 2\mathrm{e}^{-\hat{\sigma}_1/3}\mathrm{e}^{-2\hat{\sigma}_1\delta} = 0$$

Dropping the second term on the right-hand side in the large-ρ limit and solving for δ we deduce that for sufficiently large ρ,

$$x_0 \approx \frac{1}{3} - \frac{\ln 2}{3\rho\sigma_{\mathrm{I}}}$$

Hence, $x_0 \to 1/3, x_1 \to 2/3$ in the limit $\rho \to \infty$. In Fig. 5, we plot $\Lambda_\rho(x)$ for a range of values of ρ with $L_0 = 1$ and fixed weight parameters $\sigma_{\mathrm{E,I}}, \beta$. The bump is stable provided that the function $\Lambda_\rho(x)$ only crosses the x-axis at the points $x = x_0, x_1$. The behavior of Λ_ρ as a function of ρ is similar to that of the front. That is, as ρ increases, zero crossings occur close to the boundary of the domain. The function $\Lambda_\rho(x)$ also develops additional stationary points so that as ρ is further increased, these points also cross the x-axis leading to additional regions of instability. Again these latter crossings generate the splitting of ocular dominance columns via frequency-tripling as illustrated in Fig. 6, where we show the evolution of an unstable bump for the fixed values of ρ corresponding to Fig. 5(b and c).

3.3. Periodic pattern

It is instructive to extend the above analysis to the case of a spatially periodic solution of the Swindale model defined on the unbounded domain $-\infty < x < \infty$:

$$\frac{\partial n}{\partial t} = [1 - n(x,t)^2]\left[\int_{-\infty}^{\infty} W(|x - x'|)n(x',t)\,\mathrm{d}x'\right]. \tag{48}$$

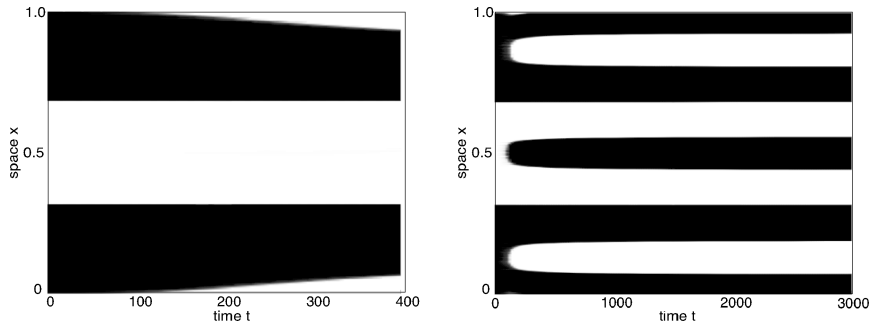

Fig. 6 Evolution of an unstable stationary bump for fixed ρ. Other parameter values as in Fig. 5. (a) $\rho = 7.2$: insertion of new columns at the boundary. (b) $\rho = 8$: frequency-tripling in which each column splits into three alternating columns.

Such a multi-bump solution is of the form

$$\bar{n}(x) = \sum_{m=-\infty}^{\infty} (-1)^m H_m(x), \tag{49}$$

where

$$H_m(x) = \begin{cases} 1, & \text{if } md < x < (m+1)d \\ 0, & \text{otherwise} \end{cases}$$

with d being the characteristic width of each bump. Linearizing about $\bar{n}$ leads to Eq. (27) with $\Lambda_\rho \to \Lambda^*$, where

$$\Lambda^*(x) = \left(\int_{-\infty}^{\infty} W(|x - x'|)\bar{n}(x')\,\mathrm{d}x' \right). \tag{50}$$

The periodic pattern is stable provided that $\bar{n}(x)\Lambda^*(x) > 0$ for all $x \in (-\infty, \infty)$. Substituting Eqs. (16) into Eq. (50) shows that $\Lambda^*(x) = \Phi_{\sigma_\mathrm{E}}(x) - \beta\Phi_{\sigma_\mathrm{I}}(x)$ with

$$\Phi_\sigma(x) = \int_{-\infty}^{x} \mathrm{e}^{\sigma(x'-x)}\bar{n}(x')\,\mathrm{d}x' + \int_{x}^{\infty} \mathrm{e}^{\sigma(x-x')}\bar{n}(x')\,\mathrm{d}x'. \tag{51}$$

Let us calculate $\Phi_\sigma(x)$ on the interval $md < x < (m+1)d$. Substituting for $\bar{n}$ using Eq. (49) leads to the decomposition

$$\Phi_\sigma(x) = \sum_{n=-\infty}^{m-1} (-1)^n \int_{nd}^{(n+1)d} \mathrm{e}^{\sigma(x'-x)}\,\mathrm{d}x' + \sum_{n=m+1}^{\infty} (-1)^n \int_{nd}^{(n+1)d} \mathrm{e}^{\sigma(x-x')}\,\mathrm{d}x'$$
$$+(-1)^m \left[\int_{md}^{x} \mathrm{e}^{\sigma(x'-x)}\mathrm{d}x' + \int_{x}^{(m+1)d} \mathrm{e}^{\sigma(x-x')}\mathrm{d}x' \right].$$

Evaluating each of these integrals and summing the resulting geometric series gives

$$\Phi_\sigma(x) = \frac{2}{\sigma}(-1)^m \left[1 - \frac{e^{\sigma((m+1)d-x)} + e^{\sigma(x-md)}}{1+e^{\sigma d}}\right], \quad md < x < (m+1)d.$$

Setting $y = x - md$ and noting that $\bar{n}(x) = (-1)^m$ over the interval $md < x < (m+1)d$, we deduce that

$$\bar{n}(y+md)\Phi_\sigma(y+md) = \Psi_\sigma(y), \quad 0 < y < d \tag{52}$$

with

$$\Psi_\sigma(y) = \frac{2}{\sigma}\left[1 - \frac{\cosh(\sigma(y-d/2))}{\cosh(\sigma d/2)}\right]. \tag{53}$$

The function $\Psi_\sigma(y)$ is a positive, unimodal function that is symmetric about its maximum at $y = d/2$. Since the right-hand side of Eq. (52) is independent of m, we conclude that the periodic pattern is stable provided that

$$\Psi(y) \equiv \Psi_{\sigma_E}(y) - \beta\Psi_{\sigma_I}(y) > 0, \quad 0 < y < d. \tag{54}$$

We now show that if inhibition is sufficiently strong then only patterns up to a critical width d_c are stable. Equation (53) gives $\Psi(0) = 0$ and

$$\Psi'(0) = \tanh(\sigma_E d/2) - \beta\tanh(\sigma_I d/2) > 0,$$

which follows from the lateral inhibition conditions $\sigma_E > \sigma_I$ and $0 < \beta < 1$. Hence, $\Psi(y)$ is a positive, increasing function sufficiently close to the boundaries $y = 0, d$. It will remain positive unless $\Psi(d/2) < 0$. In the case of small d, we have

$$\Psi(d/2) \approx \frac{d^2}{8}(\sigma_E - \beta\sigma_I) > 0,$$

whereas for large d

$$\Psi(d/2) \approx \frac{1}{\sigma_E} - \frac{\beta}{\sigma_I} < 0,$$

assuming that $\sigma_E > \sigma_I/\beta$. The latter condition is equivalent to requiring that the Fourier transform of $W(x)$ satisfy $\widetilde{W}(0) < 0$. One finds that there exists a critical value of width d_c for which $\Psi(d_c/2) = 0$ such that $\Psi(d/2) > 0$ for $d < d_c$ and $\Psi(d/2) < 0$ for $d > d_c$. This is illustrated in Fig. 7. Our analysis is consistent with the Turing-like approach to analyzing the Swindale model (Swindale, 1980). That is, linearizing about the homogeneous binocular state, one finds that for $\sigma_E > \sigma_I/\beta$ there exists a semi-infinite band of eigenmodes that grow to form a periodic pattern (see Fig. 2). These modes are the ones with a sufficiently high wave number k, which corresponds to small values of d.

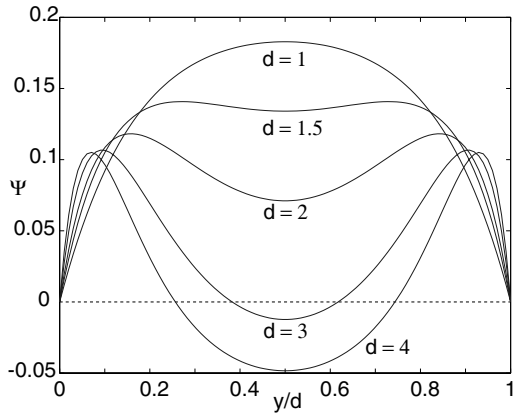

Fig. 7 Plot of $\Psi(y)$ for various values of width d in the case of a periodic pattern. The parameters of the weight distribution (16) are taken to be $\beta = 0.5, \sigma_E = 4.4, \sigma_I = 1.9$.

4. Numerical results

In this section, we describe numerical results obtained by directly simulating the one-dimensional model evolving according to Eq. (11), and interpret our results in terms of the analysis presented in Section 3. Note that we include the slowly varying term $(\dot{\rho}/\rho)n$ in our simulations, although the model produces similar results without it. We assume slow logistic growth with $\rho(t)$ given by Eq. (23) for $\epsilon \ll 1$. We consider two types of initial condition. The first consists of a stable front solution, which exists provided that the initial length L_0 is sufficiently small; this allows us to make a direct comparison with the analysis of Section 3. The second consists of a binocular state at a larger value of L_0, which immediately undergoes a Turing instability leading to the formation of an ocular dominance column pattern; this is the more likely situation from a developmental perspective. The subsequent progression of the pattern as the domain size grows exhibits two distinct time scales: the slow widening of the columns as the length of the domain increases, and the rapid transitions that occur when the system becomes unstable, quickly followed by the insertion of new ocular dominance columns. We take into account these two time scales by using an adaptive-step numerical scheme. That is, we take relatively large time steps, unless the value of the next step determined by Euler's Method significantly differs from the value predicted by Improved Euler's. In the latter case, we continually halve the time step until the two predictions are within a given tolerance.

First, suppose that the initial state is a stable front solution (small L_0). With free boundary conditions, the stability analysis from Section 3.1 indicates that this solution will remain stable until the cortex reaches some critical length, at which point columns will be inserted at the boundaries. In line with Fig. 3(b), we find numerically that this occurs at a critical length $L = \rho L_0 \approx 4$. We also find that as the cortex continues to grow, frequency-tripling bifurcations occur in the interior of the domain, resulting in the formation of a multiple stripe pattern, see Fig. 8(a). Associated with each column insertion is a sharp reduction in the mean width of an ocular dominance column and a transient rise in the corresponding variance. This

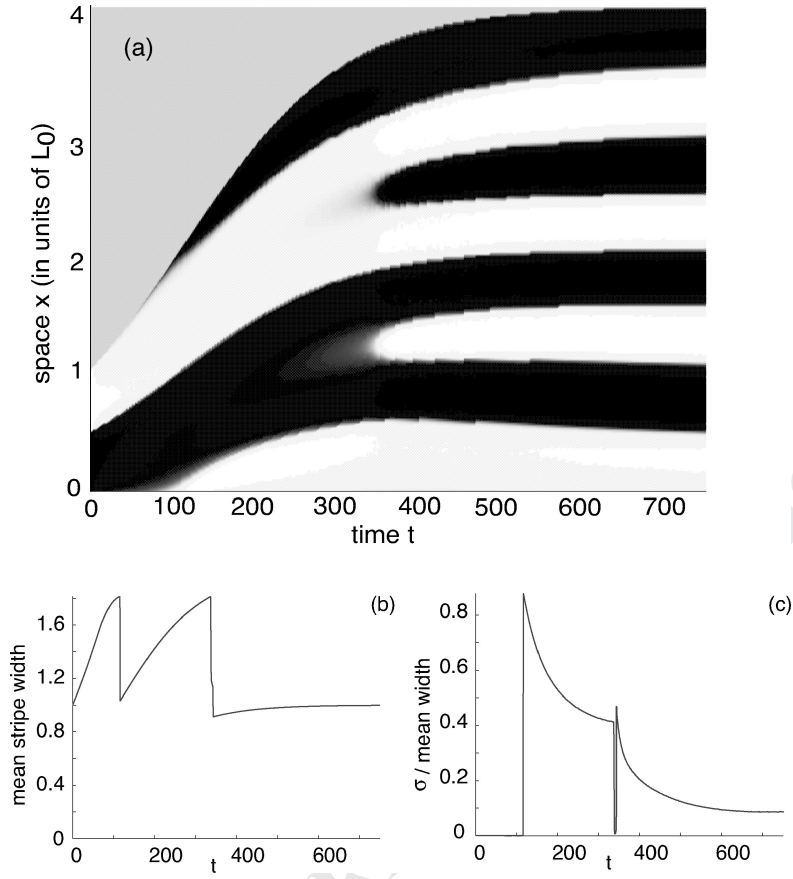

Fig. 8 (a) A plot of the growth from a front pattern at an initial length $L_0 = 2$ under logistic growth with $\epsilon = 0.01$ and $\xi = 4$. The parameters of the weight distribution (16) are taken to be $\beta = 0.5, \sigma_E = 4.4, \sigma_I = 1.9$ and $A = 10$. White corresponds to left eye dominance and black corresponding to right eye dominance. (b) The mean ocular dominance column width against time. (c) The standard deviation σ of the ocular dominance width against time.

is shown in Fig. 8(b and c). Note that not all of the ocular dominance columns split at exactly the same time. This pattern irregularity is a consequence of the boundary instabilities. However, this may not be a defect of the model, since the ocular dominance patterns observed experimentally also tend to be rather disordered (Hubel and Wiesel, 1977; Swindale, 1996). A much more regular pattern can be generated by using periodic boundary conditions instead of free boundary conditions, as illustrated in Fig. 9. An alternative mechanism for eliminating boundary effects would be to increase the growth rate ϵ, so that the frequency-tripling bifurcation occurs before the boundary instabilities have had a chance to develop. However, this appears to require an unrealistically fast growth rate.

Now suppose that the system starts off in a binocular state (large L_0), and immediately undergoes a Turing-like instability leading to the formation of an

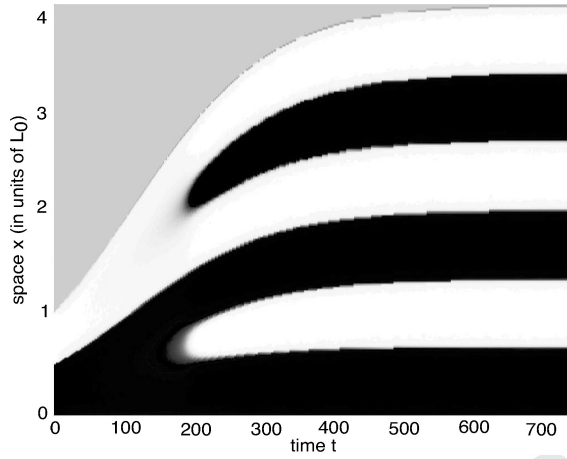

Fig. 9 Same as Fig. 8 except with periodic boundary conditions. Note the regularity of the frequency-tripling bifurcations compared to Fig. 8.

ocular dominance pattern with mean column width $d \approx \pi/k_c$, where k_c is the critical wavenumber of the associated weight distribution (16). Note that the resulting pattern, which already has a certain degree of irregularity, then undergoes both boundary insertions and frequency-tripling bifurcations as the length of the domain slowly increases, see Fig. 10. Thus, as in the previous example, frequency-tripling provides a mechanism for column insertion, whereby the mean column width is approximately preserved. This is consistent with the recent experimental finding that the column width in adult cats is similar to that of kittens, even though the cortex has at least doubled in size (Rathjen et al., 2003). In our simulations we find that frequency-tripling bifurcations occur when the domain size has increased by a factor of 2.5–3 from when ocular dominance columns first form. This is only a slight over estimate of postnatal growth in cat, particularly given the simplicity of the model. Our model actually makes the stronger prediction that if the mean column width were sampled more frequently during postnatal development, then one would detect two distinct regimes: one characterized by a slow increase in column width and the other characterized by a relatively sharp decrease in width due to column insertions. Finally, note that our basic results are robust to changes in the various weight parameters and to changes in the rate of growth. The same qualitative behavior is also seen in another well-known developmental model as shown below.

5. Correlation-based Hebbian model

For simplicity, we have formulated the problem of ocular dominance column formation on a growing cortical domain in terms of Swindale's developmental model (Swindale, 1980). One possible limitation of this particular model is its assumption that opposite eye interactions are anti-correlated. It turns out, however, that the results of our analysis carry over to another well-known developmental model, namely the correlation-based linear Hebbian model with subtractive normalization (Miller et al., 1989). We first describe the construction of the model on a fixed cortical domain. Let $n_L(\mathbf{r})$ and $n_R(\mathbf{r})$ denote the synaptic densities of feedforward

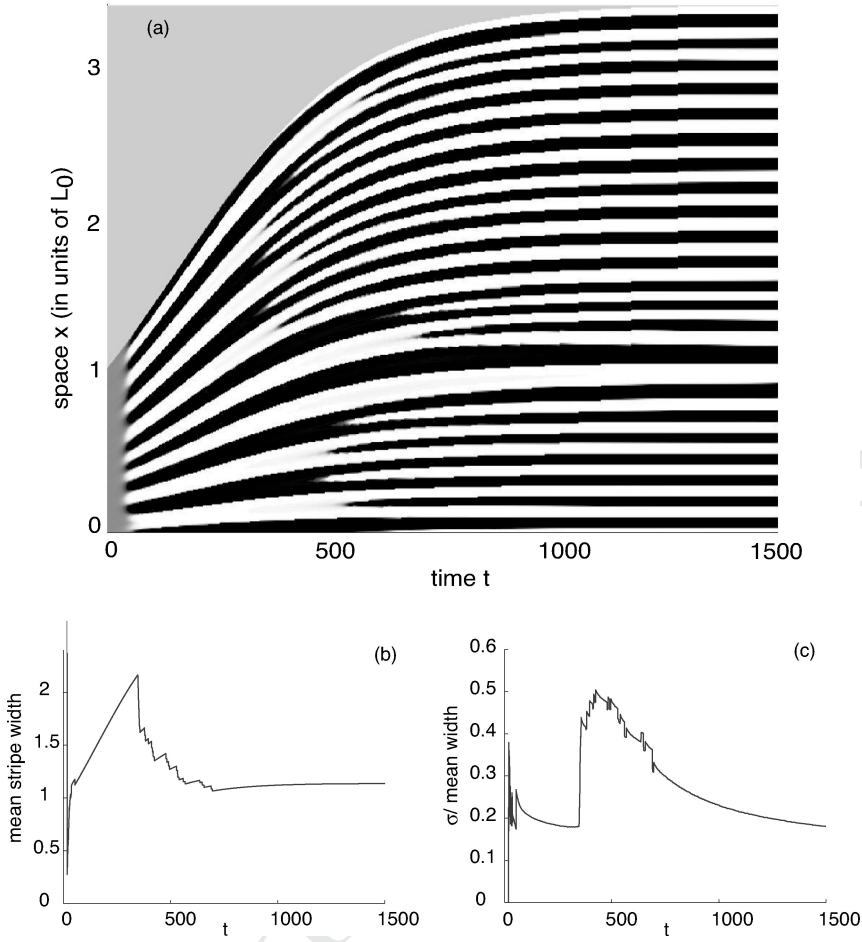

Fig. 10 (a) A plot of the growth from a binocular state at an initial length $L_0 = 16$ under logistic growth with $\epsilon = 0.005$ and $\xi = 3.2$. Other parameter values as in Fig. 8. White corresponds to left eye dominance and black corresponding to right eye dominance. (b) The mean ocular dominance column width against time. (c) The standard deviation σ of the ocular dominance width against time.

afferents from the left and right eyes to a point $\mathbf{r}$ in cortex; for the moment these are assumed to be fixed as well. Suppose that there are also weak intracortical synaptic interactions between neurons at $\mathbf{r}$ and $\mathbf{r}'$ given by the distribution $J(|\mathbf{r} - \mathbf{r}'|)$. Assuming a linear model for the cortical activity $V(\mathbf{r}, t)$ at time t, we take

$$\tau_0 \frac{\partial V(\mathbf{r}, t)}{\partial t} = -V(\mathbf{r}, t) + \int_\Omega J(\mathbf{r} - \mathbf{r}')V(\mathbf{r}', t)\,\mathrm{d}\mathbf{r}' + n_\mathrm{L}(\mathbf{r})I_\mathrm{L}(\mathbf{r}) + n_\mathrm{R}(\mathbf{r})I_\mathrm{R}(\mathbf{r}), \tag{55}$$

where τ_0 is a membrane time constant and $I_{\rm L}(\mathbf{r})$ and $I_{\rm R}(\mathbf{r})$ denote left and right eyes inputs. These inputs are generated at random from some given probability distribution that characterizes the input statistics. Since development takes place on a much slower time-scale than the dynamics of cortical activity, we can take V to be given by its steady-state value. Calculating this steady-state requires inverting the linear operator $\widehat{L}V(\mathbf{r}) = V(\mathbf{r}) - \int J(|\mathbf{r}-\mathbf{r}'|)V(\mathbf{r}')\,{\rm d}\mathbf{r}'$. In the case of weak cortical interactions, this inversion can be carried out by performing a perturbation expansion in J. The first order approximation is thus

$$V(\mathbf{r}) = \int_\Omega M(|\mathbf{r}-\mathbf{r}'|)\left[n_{\rm L}(\mathbf{r}')I_{\rm L}(\mathbf{r}') + n_{\rm R}(\mathbf{r}')I_{\rm R}(\mathbf{r}')\right]{\rm d}\mathbf{r}' \tag{56}$$

with $M(r) \approx \delta(r) + J(r)$ and δ is the Dirac delta function. Given the steady-state response to an input for fixed synaptic densities $n_{\rm L}, n_{\rm R}$, we now allow these densities to vary slowly in time according to a Hebbian rule with subtractive normalization (Miller et al., 1989):

$$\tau\frac{\partial n_{\rm L}}{\partial t} = \langle VI_{\rm L}\rangle - \gamma(\mathbf{n}), \qquad \tau\frac{\partial n_{\rm R}}{\partial t} = \langle VI_{\rm R}\rangle - \gamma(\mathbf{n}), \tag{57}$$

where $\tau \gg \tau_0$, $\langle\ldots\rangle$ denotes averaging over the distribution of inputs $I_{\rm L,R}$, and the decay term $\gamma(\mathbf{n})$ enforces a conservation constraint.

Suppose that the input correlations are of the form

$$\begin{pmatrix} \langle I_{\rm L}(\mathbf{r})I_{\rm L}(\mathbf{r}')\rangle & \langle I_{\rm L}(\mathbf{r})I_{\rm R}(\mathbf{r}')\rangle \\ \langle I_{\rm R}(\mathbf{r})I_{\rm L}(\mathbf{r}')\rangle & \langle I_{\rm R}(\mathbf{r})I_{\rm R}(\mathbf{r}')\rangle \end{pmatrix} = Q(\mathbf{r}-\mathbf{r}')\mathbf{C}, \qquad \mathbf{C} = \begin{pmatrix} C_{\rm S} & C_{\rm D} \\ C_{\rm D} & C_{\rm S} \end{pmatrix}, \tag{58}$$

where $Q(r)$ determines the spatial dependence of the correlations, $C_{\rm S}$ gives the same eye correlations and $C_{\rm D}$ the opposite eye correlations such that $C_{\rm D} < C_{\rm S}$. Substituting Eq. (56) into (57) then leads to the equation (on setting $\tau = 1$)

$$\frac{\partial n_i(\mathbf{r},t)}{\partial t} = \int w(|\mathbf{r}-\mathbf{r}'|)\sum_{j={\rm L,R}} C_{ij}n_j(\mathbf{r}',t)\,{\rm d}\mathbf{r}' - \gamma(\mathbf{n}) \tag{59}$$

for $i = {\rm L}, {\rm R}$, where $w(r) = M(r)Q(r)$. Comparison with Eq. (1) shows that $w_{ij}(\mathbf{r}) \to C_{ij}w(\mathbf{r})$ and the logistic multiplicative term has been replaced by a subtractive normalization constraint. The latter is now chosen so that the total synaptic density $n_{\rm L}(\mathbf{r}) + n_{\rm R}(\mathbf{r})$ is conserved at each point in cortex:

$$\gamma(\mathbf{n}) = \mu\int w(|\mathbf{r}-\mathbf{r}'|)\left[n_{\rm L}(\mathbf{r}) + n_{\rm R}(\mathbf{r})\right]{\rm d}\mathbf{r}' \tag{60}$$

with μ specified below. Exploiting the fact that the input correlation matrix $\mathbf{C}$ has eigenvalues $\mu_\pm = C_{\rm S} \pm C_{\rm D}$ with corresponding eigenvectors $\mathbf{e}_\pm = (1, \pm 1)$, it is straightforward to show that Eq. (59) reduces to the pair of equations

$$\frac{\partial N(\mathbf{r},t)}{\partial t} = (C_{\rm S} + C_{\rm D} - 2\mu)\int_\Omega w(|\mathbf{r}-\mathbf{r}'|)N(\mathbf{r}',t)\,{\rm d}\mathbf{r}', \tag{61}$$

$$\frac{\partial n(\mathbf{r},t)}{\partial t} = (C_S - C_D)\int_\Omega w(|\mathbf{r}-\mathbf{r}'|)n(\mathbf{r}',t)\mathrm{d}\mathbf{r}' \tag{62}$$

with $N = n_L + n_R$ and $n = n_L - n_R$. (Take the inner product of Eq. (59) with $\mathbf{e}_\pm$.) Finally, setting $\mu = (C_S + C_D)/2$, we see that the subtractive constraint ensures a constant total density N. In the absence of such a constraint ($\mu = 0$), one would require negative correlations $C_D = -C_S$ in order to conserve the total denisty, which correponds to the anti-correlation assumption of the Swindale model.

One can now proceed along identical lines to Section 2. First, we derive a single equation for the density $n = n_L - n_R$ on a growing cortical domain, which is given by Eq. (6) with

$$\mathcal{F}_t[n](\mathbf{r},t) = (C_S - C_D)\int_{\Omega_t} w_t(|\mathbf{r}-\mathbf{r}'|)n(\mathbf{r}',t)\,\mathrm{d}\mathbf{r}'. \tag{63}$$

In order to have bounded solutions, it is necessary to supplement the linear equation with the external constraints $|n(\mathbf{r},t)| \leq N$ for all $x \in \Omega_t$. Second, restricting ourselves to a one-dimensional network, we map back to a fixed domain of length L_0 to obtain the analog of Eq. (18):

$$\frac{\partial n}{\partial t} = (C_S - C_D)\int_0^{L_0} W_\rho(|x-x'|)n(x',t) - n(x,t)\frac{\dot\rho}{\rho}. \tag{64}$$

The interesting point to note is that this equation (on dropping the dilution term) together with the constraint $|n(x,t)| \leq N$ has precisely the same set of steady-state solutions (26) as the Swindale model. Moreover, they have the same stability conditions. That is, an equilibrium solution $\bar n(x)$ is stable on $x \in [0, L_0]$ provided that

$$\int_0^{L_0} W_\rho(|x-x'|)\bar n(x')\,\mathrm{d}x' > 0, \quad \text{for } \bar n(x) = N, \tag{65}$$

$$\int_0^{L_0} W_\rho(|x-x'|)\bar n(x')\,\mathrm{d}x' < 0, \quad \text{for } \bar n(x) = -N. \tag{66}$$

This is identical to the condition for (marginal) stability derived in Section 3 for the Swindale model, see Eq. (29). Thus we expect the correlation-based model to exhibit the same type of frequency-tripling bifurcations, which is confirmed numerically in Fig. 11.

6. Discussion

Most activity-dependent models for the development of ocular dominance columns have focused on the emergence of a steady-state ocular dominance pattern via a Turing-like instability from a homogeneous binocular state (Swindale, 1996). The mean width of the columns in the steady-state is determined by the critical wavenumber of the underlying intracortical weight function. Since the basic pattern forming mechanism is highly nonlinear, bifurcation methods cannot be

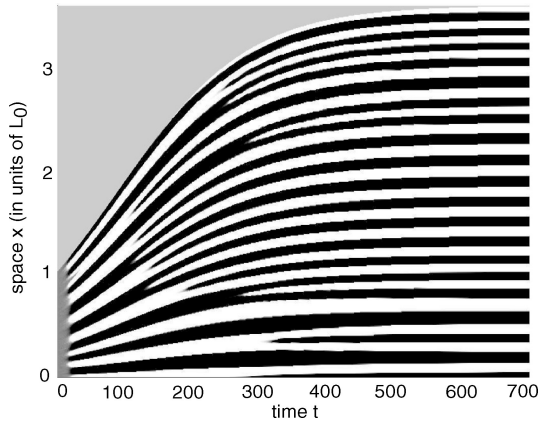

Fig. 11 A plot of the growth from a binocular state for the subtractive normalization model under logistic growth with $\epsilon = 0.01$ and $\xi = 3.5$. Here $C_S = 1$, $C_D = 0.2$, $A = 25$, and all other parameter values as in Fig. 10.

used to determine the amplitude and stability of the emerging pattern, and thus cannot be used to investigate whether or not additional instabilities occur during subsequent cortical growth. In this paper, we have shown that in the case of two well-known developmental models (Swindale, 1980; Miller et al., 1989), it is possible to analyze how stability depends on domain size by directly linearizing about the steady-state ocular dominance pattern. In one spatial dimension, we have combined this stability analysis with numerical simulations to demonstrate how changes in the size of the domain can induce one or more frequency-tripling bifurcations resulting in the insertion of new ocular dominance columns. Our model thus predicts that there are two distinct regimes of columnar growth, one characterized by a slow increase in column width and the other characterized by a relatively sharp decrease in width due to column insertions. This is consistent with the recent experimental finding that the ocular dominance column width of kittens and adult cats are comparable even though the cortex has doubled in size during postnatal growth (Rathjen et al., 2003).

There are a number of interesting issues raised by this work that warrant further investigation. The first concerns how the intracortical interaction function scales with the size of the cortex. One of the basic results of our analysis is that a simple elongation of the recurrent interactions as the cortex grows will not induce any pattern transitions (the "balloon effect"). Motivated by experimental data regarding the refinement of patchy horizontal connections during postnatal growth (Luhmann et al., 1990; Callaway and Katz, 1991), we made the simple ansatz that the interaction function is actually invariant with respect to the size of cortex; changing such a scaling rule would modify the rate at which column insertions occur. An alternative to this rather ad hoc approach would be to construct a more detailed model that considers the joint development of feedforward afferents and intracortical connections. A second important issue concerns the effects of the boundaries. In the case of free boundary conditions and slow cortical growth, our one-dimensional model predicts that additional columns are inserted at the boundaries of the domain leading to a more irregular sequence of frequency-tripling bifurcations. Boundary effects are also likely to be important in the more realistic two-dimensional case. Indeed, one finds experimentally that ocular dominance

columns tend to run orthogonally to the boundary separating primary visual cortex (V1) from extrastriate area V2. However, extending our stability analysis to two dimensions is nontrivial, particularly given the greater complexity of two-dimensional ocular dominance patterns due to the extra rotational degree of freedom (assuming isotropic lateral interactions). Such complexity is manifested by the striking differences between the stripe-like patterns found in primates and the blob-like patterns found in cat. Finally, it would be interesting to use the methods outlined in this paper to construct developmental models that take into account cortical growth during the formation of other cortical features maps such as orientation preference. Indeed, the insertion of a set of ocular dominance columns could coincide with the insertion of a corresponding set of hypercolumns. The hypercolumn is the basic functional unit of cortex that includes the full range of orientation preferences as well as a pair of left/right ocular dominance columns.

References

Callaway, E.M., Katz, L.C., 1991. Effects of binocular deprivation on the development of clustered horizontal connections in cat striate cortex. Proc. Natl. Acad. Sci. U.S.A. 88, 745–749.

Chaplain, M.A.J., Ganesh, M., Graham, I.G., 2001. Spatio-temporal pattern formation on spherical surfaces: Numerical simulation and application to solid tumor growth. J. Math. Biol. 42, 387–423.

Crair, M.C., Horton, J.C., Antomini, A., Stryker, M.P., 2001. Emergence of ocular dominance columns in cat visual cortex by two weeks of age. J. Comp. Neurol. 430, 235–249.

Crampin, E.J., Gaffney, E.A., Maini, P.K., 1999. Reaction and diffusion on growing domains: Scenarios for robust pattern formation. Bull. Math. Biol. 61, 1093–1120.

Crampin, E.J., Gaffney, E.A., Maini, P.K., 2002. Mode-doubling and tripling in reaction–diffusion patterns on growing domains: A piecewise linear model. J. Math. Biol. 44, 107–128.

Crowley, J.C., Katz, L.C., 2000. Early development of ocular dominance columns. Science 290, 1321–1324.

Duffy, K.R., Murphy, K.M., Jones, D.G., 1998. Analysis of the postnatal growth of visual cortex. Vis. Neurosci. 15, 831–839.

Ermentrout, G.B., Cowan, J.D., 1980. Secondary bifurcations in neuronal nets. SIAM J. Appl. Math. 39, 323–340.

Harris, A.E., Ermentrout, G.B., Small, S.L., 2000. A model of ocular dominance column development by competition for trophic factor: Effects of excess trophic factor with monocular deprivation and effects of antagonist of trophic factor. J. Comput. Neurosci. 8, 227–250.

Hubel, D.H., Wiesel, T.N., 1977. Functional architecture of macaque monkey visual cortex. Proc. R. Soc. Lond. B 198, 1–59.

Kondo, S., Asai, R., 1995. A reaction–diffusion wave on the skin of the marine angelfish *pomacanthus*. Nature 376, 765–768.

Luhmann, H.J., Singer, W., Martinez-Millan, L., 1990. Horizontal interactions in cat striate cortex: I. Anatomical substrate and postnatal development. Eur. J. Neurosci. 2, 344–357.

Miller, K.D., Keller, J.B., Stryker, M.P., 1989. Ocular dominance column development: Analysis and simulation. Science 245, 605–614.

Murray, J.D., 2002. Mathematical Biology, 3rd ed. Springer-Verlag, Berlin.

Painter, K.J., Maini, P.K., Othmer, H.G., 1999. Stripe formation in juvenille *Pomacathus* explained by a generalized Turing mechanism with chemotaxis. Proc. Natl. Acad. Sci. U.S.A. 96, 5549–5554.

574 Purves, D., LaMantia, A., 1993. Development of blobs in the visual cortex of macaques. J. Comp.
575 Neurol. 334, 169–175.
576 Rathjen, S., Schmidt, K.E., Lowel, S., 2003. Postnatal growth and column spacing in cat primary
577 visual cortex. Exp. Brain Res. 149, 151–158.
578 Schmidt, K.E., Galuske, R.A.W., Singer, W., 1999. Matching the modules: Cortical maps and long-
579 range connections in visual cortex during development. J. Neurobiol. 41, 10–17.
580 Shatz, C.J., Luskin, M., 1986. The relationship between the geniculocortical afferents and their
581 cortical target cells during development of the cat's primary visual cortex. J. Neurosci. 6,
582 3655–3668.
583 Swindale, N.V., 1980. A model for the formation of ocular dominance stripes. Proc. R. Soc. B 208,
584 243–264.
585 Swindale, N.V., 1996. The development of topography in visual cortex: A review of models. Net-
586 work: Comp. Neural Syst. **7**, 161–247.
587 Turing, A.M., 1952. The chemical basis of morphogenesis. Phil. Trans. R. Soc. Lond. B 237, 32–72.
588 Varea, C., Aragon, J.L., Barrio, R.A., 1997. Confined Turing patterns in growing systems. Phys.
589 Rev. E 56, 1250–1253.

Queries to Publisher:

P1: Pub: Please provide the acceptance information for this article.

Queries to Author:

A1: Au: Please check the corresponding author for correctness.

A2: Au: Please provide a list of 3–4 key words for this article.